Origins of asymmetric charge transport properties of weakly coupled molecular junctions

Dexian Sun,[1] Li Li,[1] Xi Yu,[2] and Guangjun Tian[1,*]

[1]*Key Laboratory for Microstructural Material Physics of Hebei Province, School of Science, Yanshan University, Qinhuangdao 066004, China*

[2]*Tianjin Key Laboratory of Molecular Optoelectronic Science, Department of Physics, School of Science, Tianjin University, Tianjin 300072, China*

(Received 29 October 2018; revised manuscript received 15 February 2019; published 22 March 2019)

Understanding charge transport properties of a molecular junction plays a crucial role in the possible application of such devices. In this work we present a theoretical study on the transport properties of molecular transistors in the sequential tunneling regime. Special attention is paid to the origins of the asymmetries in the charge transport properties as presented by the commonly measured conductance stability diagrams (two-dimensional plots of the differential conductance against gate and bias voltages). It is found that both the *external* factors, including the bias coupling constant and the coupling strength between the molecule and the electrodes, and the *intrinsic* molecular properties such as the frequency differences between different charging states, the anharmonicity of the potential energy surface, and the mode-mixing effect can lead to asymmetric conductance stability diagrams. Especially, we show that the uneven bias coupling between the molecule and the two electrodes can result in strong current rectifications. These results successfully reproduce the change in rectification directions of molecular diodes as observed in a recent experiment [L. Yuan *et al.*, Nat. Commun. **6**, 6324 (2015)]. The differences in the asymmetric stability diagram caused by the studied factors are also discussed, which helps us to correctly interpret the experimental results.

DOI: 10.1103/PhysRevB.99.125423

I. INTRODUCTION

Molecular junctions are tiny devices in which molecules are connected to electrodes to form electric circuits. Such systems are often considered to be one of the promising building blocks for future electronic devices and have been extensively studied both experimentally and theoretically in the past two decades [1–8]. The rapid development of experimental techniques has also made molecular junctions an important test bed for fundamentally important problems such as the interaction of charge carriers and the nuclear motions of the molecules during the charge transport process. Especially, the charge transport properties of single-molecule transistors as designed as an analog to the classical field effect transistors have been measured to extremely high precision, which has led to the observation of many interesting phenomena such as the excitation of molecular vibrations [9–12] and the suppression of the low-bias current by strong electron-vibration couplings (Franck-Condon blockade) [7,8,13]. The charge transport properties of single-molecule transistors are normally measured as functions of both the source-drain bias voltage and the gate voltage and presented as two-dimensional plots of the differential conductance as functions of the bias and gate voltages (known as the conductance stability diagram or Coulomb diamond). From the conductance stability diagrams, much important information about the electron transport properties of the molecular transistor can be obtained, including the charging energies of different charging states, the vibrational modes, and vibrational progressions of the conducting state. However, because the transport property of a single-molecule transistor can be affected by many factors such as the molecule-electrode coupling strength, the bias and gate couplings, and the intrinsic properties of the molecule itself, the resulting conductance stability diagrams could be rather complicated to interpret, which thus causes difficulties in the unambiguous determination of the properties of interest.

To address such a problem, we present in this work a systematic theoretical study of the charge transport properties of a single molecule weakly coupled to the metallic electrodes. The charge transport through the molecule is assumed to be dominated by one spin-degenerate quantum level. The electronic transport properties of such weakly coupled molecular junctions were described by performing rate equation calculations in the sequential tunneling regime [14–18]. Special attention is paid to the possible origins of the asymmetry in the conductance stability diagrams of the system, which could supply helpful guidance for the interpretation of the experimental results. Moreover, we also show that strong current rectifications can be obtained when the bias couplings between the molecule and the source and drain electrodes are not equal. Depending on the ratio of the bias couplings, the direction of the current rectification can also be tuned, which nicely reproduces the change in the rectification directions of molecular diodes, as observed in a recent experiment by Yuan *et al.* [19].

The rest of the paper is organized as follows: in Sec. II we introduce the model and theoretical method we used to simulate the single-molecule transistor and its transport properties. The influences of various factors on the charge

*tian@ysu.edu.cn

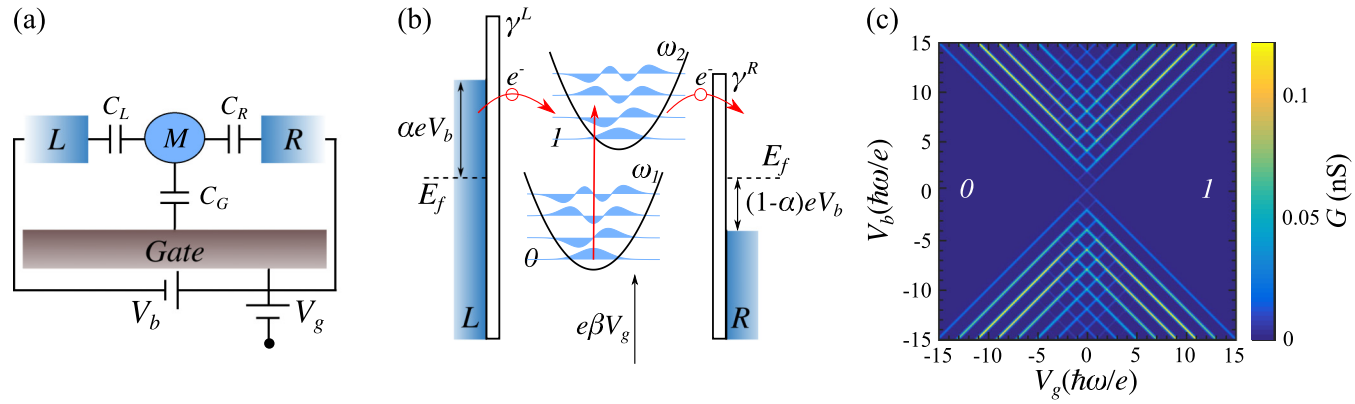

FIG. 1. (a) Schematic drawing of the single-molecule transistor studied in the present work. The molecule (M) was capacitively coupled to the left (L), right (R), and gate electrodes with the corresponding electrode capacitances C_L, C_R, and C_G [14]. (b) The corresponding energetic diagrams of the transistor. The molecule is represented by two charging states ($|0\rangle$ and $|1\rangle$), each with a number of vibrational levels. (c) A typical symmetric conductance stability diagram computed for harmonic potentials with $\alpha = \beta = 0.5$, $\omega_1 = \omega_2 = 1000\,\mathrm{cm}^2$, $\gamma^L = \gamma^R = 1.0\,\mu\mathrm{eV}$, $\Delta Q = 41.90$ a.u.

transport properties of the model transistor are presented in Sec. III together with corresponding discussions. Section IV gives a summary of the work.

II. MODEL AND THEORETICAL METHOD

A. Model

A schematic picture of the single-molecule transistor considered in this work and the corresponding energetic diagrams are shown in Figs. 1(a) and 1(b), respectively. The molecule (M) was assumed to weakly coupled to the left (L) and right (R) electrodes which act as electron reservoirs. In the weak-coupling limit, the transport is dominated by sequential tunneling where the charge carrier can stay on the molecule for a time sufficiently long to lose coherence [20]. As a result, the molecule undergoes charging and decharging during the charge transport process [schematically shown by the vertical red arrow in Fig. 1(b)]. For the sake of simplicity, we consider only two electronic charging states, an electron unoccupied state $|0\rangle$ and an occupied state $|1\rangle$, in the following discussion. Such a treatment is equivalent to the assumption that the transport through the molecule is dominated by a single spin-degenerate conducting channel under the Coulomb blockade condition [15].

The influences of the bias and gate voltages on the molecule were included by the capacitance of the molecule to the electrodes (C_L, C_R, and C_G) [14,16]. Charge transport can take place when the conducting channel enters the potential window between the left and right electrodes as opened up by applying a bias voltage V_b, as shown in Fig. 1(b). In order to facilitate the discussion, we assume the energy difference between the conducting channel and the Fermi energy of the electrodes E_f is ϵ_0. In the electronic state picture, ϵ_0 can be considered effectively as the energy difference between electronic states $|1\rangle$ and $|0\rangle$. It should be noted here that we have neglected the internal relaxations and the interactions between electrons in different energy levels [14]. The energy of the electrons in the reservoirs should exceed ϵ_0 for the charge transport to happen. A gate voltage can be introduced to tune the relative position of the conducting channel with respect to E_f. Under a gate voltage of V_g, the energy difference between the conducting channel and E_f can then be written as $\epsilon = \epsilon_0 - e\beta V_g$, with $\beta = C_G/(C_L + C_R + C_G)$ being the gate coupling constant [14–16]. The effect of the gate voltage can also be understood from the electronic states' point of view. In fact, electronic states with different numbers of electrons will respond differently to the gate voltages [14,21]. As a result, the energy difference between the two states will also be affected by the applied gate voltage. This change is equivalent to the energy shift of the conducting channel caused by the gate voltage. In the simulations we have assumed $\epsilon_0 = 0$, i.e., the conducting channel is aligned with E_f at $V_g = 0$ (or, equivalently, the energy difference between the two states is zero), which thus allows the charge transport to happen as long as nonzero bias voltages are applied. Such a condition can be met by applying a reference gate voltage of $V_{g0} = \epsilon_0/e\beta$ [14].

In order to take into account the electron-vibration coupling effect, each state is associated with vibrational modes described by given potential energy surfaces (PESs). In the following simulations, we consider only one harmonic vibrational mode for each state unless otherwise stated. The equilibrium positions of the corresponding PESs belonging to different charging states were shifted by ΔQ to include vibrational excitations.

The Hamiltonian describing the model molecular transistor outlined above can be written as [15,22–24]

$$H = H_M + H_E + H_V. \tag{1}$$

Here H_M, H_E, and H_V represent the Hamiltonians of the molecule, the two electron reservoirs, and the coupling between the molecule and the reservoirs, respectively. The molecular Hamiltonian can be written as [22,23]

$$H_M = \sum_l \epsilon_{0,l} |0,l\rangle\langle 0,l| + \sum_{l'} \epsilon_{1,l'} |1,l'\rangle\langle 1,l'|. \tag{2}$$

Here the eigenvalue and wave functions for the molecule can be obtained by solving the Schrödinger equation for given PESs; $|0,l\rangle$ and $|1,l'\rangle$ correspond to the vibrational levels with quantum numbers l and l' in states $|0\rangle$ and $|1\rangle$,

respectively. Under the Born-Oppenheimer approximation, $|0,l\rangle$ ($|1,l'\rangle$) can be rewritten as $|0\rangle_e \otimes |l\rangle_v$ ($|1\rangle_e \otimes |l'\rangle_v$), with $|0\rangle_e$ ($|1\rangle_e$) and $|l\rangle_v$ ($|l'\rangle_v$) being the electronic part (e) and vibrational part (v) of the wave functions, respectively. $\epsilon_{0,l}$ and $\epsilon_{1,l'}$ are the energies for the corresponding levels, and their differences are dependent on V_g as $\epsilon_{1,l'} - \epsilon_{0,l} = \epsilon^0_{1,l'} - \epsilon^0_{0,l} - e\beta V_g$ ($\epsilon^0_{1,l'}$ and $\epsilon^0_{0,l}$ are the unperturbed energies), as we have discussed above. The Hamiltonian for the two reservoirs can be written as [15,22–24]

$$H_E = \sum_{r,\mathrm{k}} \epsilon_{r\mathrm{k}} c^\dagger_{r\mathrm{k}} c_{r\mathrm{k}}, \tag{3}$$

where $r = L, R$ represent the left and right reservoirs. $c^\dagger_{r\mathrm{k}}$ and $c_{r\mathrm{k}}$ are the creation and annihilation operators of electron in the reservoir, with k being the momentum of the electron. The energy of the electron in the two reservoirs $\epsilon_{r\mathrm{k}}$ is dependent on the applied bias voltages in the way shown in Fig. 1(b). The coupling Hamiltonian that describes the tunneling of electron into and out of the molecule can be written as [15,22–24]

$$H_V = \sum_{r,\mathrm{k}} V_r (c^\dagger_{r\mathrm{k}} d + d^\dagger c_{r\mathrm{k}}). \tag{4}$$

Here $d^\dagger = |1\rangle_{ee}\langle 0|$ and $d = |0\rangle_{ee}\langle 1|$ are the creation and annihilation operators of the electronic states. V_L (V_R) describes the coupling strength between the molecule and left (right) electrode. V_r is related to the bonding condition between the molecule and the electrodes as well as the coupling between the conducting channel and the electrodes. In this work we assume that $V_L = \gamma^L$ and $V_R = \gamma^R$, as shown in Fig. 1(b).

B. Theoretical method

As we discussed above, in the weak-coupling limit considered in the present work, the charge transport of the single-molecule transistor considered is dominated by sequential tunneling. In the sequential tunneling regime, the electron transport properties of the transistor can be appropriately described in the framework of rate equations [15,16].

The occupation probability P_l for a given vibrational level l can be obtained by solving the rate equation [15–18]

$$\frac{dP_l}{dt} = \sum_{l'} (R_{ll'} + \Gamma_{ll'}) P_{l'}. \tag{5}$$

Here $R_{ll'}$ and $\Gamma_{ll'}$ are elements of matrices describing the tunneling rates and relaxations, respectively. The tunneling rates for interstate transitions between level l in the initial state $|0\rangle$ and level l' in the final state $|1\rangle$ can be computed by Fermi's golden rule as [16]

$$R_{l'l} = \frac{\gamma^L}{\hbar} f(\epsilon^L) |_v\langle l|l'\rangle_v|^2 + \frac{\gamma^R}{\hbar} f(\epsilon^R) |_v\langle l|l'\rangle_v|^2 \tag{6}$$

and

$$R_{ll'} = \frac{\gamma^L}{\hbar} [1 - f(\epsilon^L)] |_v\langle l'|l\rangle_v|^2 + \frac{\gamma^R}{\hbar} [1 - f(\epsilon^R)] |_v\langle l'|l\rangle_v|^2. \tag{7}$$

Here $f(\epsilon) = 1/(1 + e^{\epsilon/k_B T})$ is the Fermi function, which depends on the temperature T in the electrodes, and k_B is the Boltzmann constant. $\epsilon^L = \epsilon^0_{1,l'} - \epsilon^0_{0,l} - \alpha e V_b - e\beta V_g$ and $\epsilon^R = \epsilon^0_{1,l'} - \epsilon^0_{0,l} - (\alpha - 1) e V_b - e\beta V_g$ describe the relative position of the two levels and the potential window opened up by the bias voltage V_b. Here $\alpha = (C_R + C_G/2)/(C_L + C_R + C_G)$ is the bias coupling constant. $|_v\langle l|l'\rangle_v|^2 = |_v\langle l'|l\rangle_v|^2$ are the Franck-Condon factors. For simple potential energy surfaces such as harmonic potentials, the Franck-Condon factors can be computed analytically [25]. Consider the simple case of one-dimensional displaced harmonic potentials shown in Fig. 1(b), and if we assume no frequency change between these two states, i.e., $\omega_1 = \omega_2 = \omega$, then the Franck-Condon factors can be calculated from the displacement vector ΔQ and the frequency ω. It is convenient to introduce the electron-vibration coupling parameter $\lambda = \Delta Q \sqrt{\omega/2\hbar}$ to compute the Franck-Condon factors. The square of λ is known as the Huang-Rhys factor. With λ in hand, the Franck-Condon overlap for the one-dimensional displaced harmonic potentials can then be computed as [26]

$$_v\langle l|l'\rangle_v = \sqrt{l!l'!} e^{-\lambda^2/2} \sum_{k=0}^{\min(l,l')} \frac{(-1)^{l'+k} \lambda^{l+l'-2k}}{k!(l-k)!(l'-k)!}. \tag{8}$$

The diagonal elements of the rate matrix can be computed as

$$R_{ll} = -\sum_{l'=1,N}^{l' \neq l} R_{l'l}. \tag{9}$$

Here N is the total number of vibrational levels included. All of the other elements in the rate matrix are zero.

For the two-charging-state model considered here, only the matrix elements for the intrastate vibrational decay processes are nonzero. And the decay rates were modeled by a single vibrational relaxation time τ, as has been used in previous works [16–18]. For the nondiagonal terms, we have

$$\Gamma_{ll'} = \frac{1}{\tau} \frac{e^{-\epsilon_l/k_B T}}{\sum_k e^{-\epsilon_k/k_B T}}. \tag{10}$$

The second term on the right-hand side of the above expression is the equilibrium occupation probability of level l according to the Boltzmann distribution. And the summation over k runs over the vibrational levels in the charging state that vibrational levels l and l' belong to. ϵ_l and ϵ_k are the energies for the corresponding vibrational levels. For the diagonal terms, we get

$$\Gamma_{ll'} = \frac{1}{\tau} \left(\frac{e^{-\epsilon_l/k_B T}}{\sum_k e^{-\epsilon_k/k_B T}} - 1 \right). \tag{11}$$

By solving the rate equations, we can obtain the steady state of the system under given bias and gate voltages. Based on the steady-state populations, the current can be computed as

$$I = e \sum_l \sum_{l'} (P_l R_{l'l} - P_{l'} R_{ll'}). \tag{12}$$

With the current available, the conductance can then be obtained as $G = \partial I / \partial V_b$.

C. Simulation details

In the simulations we solve the rate equations by computing the null space of the matrix M containing both the tunneling rate matrix R and the decay matrix Γ as $M = R + \Gamma$ by

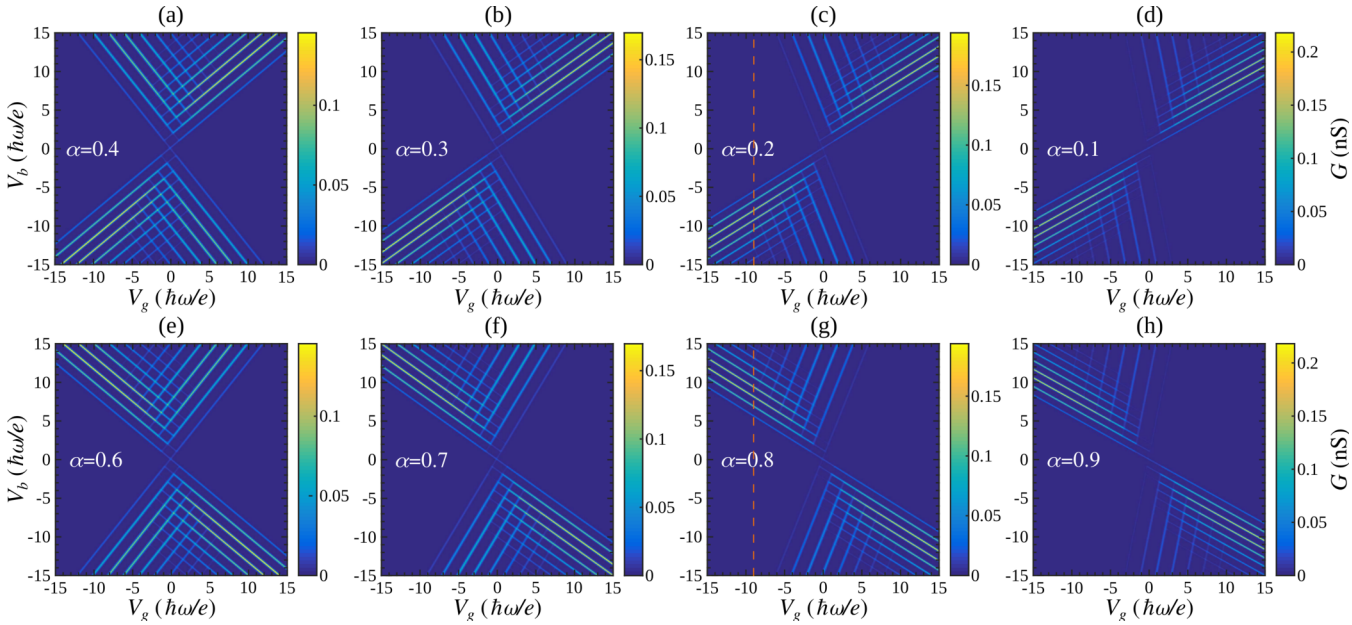

FIG. 2. Conductance stability diagrams simulated with different values of the bias coupling constant α. All of the other parameters are the same as in Fig. 1(c).

singular-value decomposition [16–18]. Sufficient vibrational energy levels were included in the calculations to guarantee the convergence of the results. The vibrational relaxation time has been set to $\tau = 1.0$ ns. The Franck-Condon factors for models with harmonic potentials were computed analytically with the DYNAVIB software [27]. For the Morse potential, the Franck-Condon factors were computed numerically by the direct integration of the corresponding vibrational wave functions [18]. All of the simulations were performed under the temperature $T = 50$ K; β has been set to 0.5 in all of the simulations presented in this work.

III. RESULTS AND DISCUSSION

A typical conductance stability diagram obtained with symmetric molecule electrode coupling ($\gamma^L = \gamma^R$), symmetric bias coupling ($\alpha = 0.5$), and the same frequency for the two charging states ($\omega_1 = \omega_2$) is shown in Fig. 1(c). The displacement ΔQ has been set to 41.90 a.u., which corresponds to $\lambda = 2$. This value of ΔQ allows us to have sufficient vibrational levels in the conductance stability diagram, which is helpful for the following discussion. It can be clearly seen that, under such ideal conditions, the conductances are symmetric with respect to both the bias and gate voltages. It is worth mentioning that the two sides with respect to the gate voltage represent different transitions. On the $V_g < 0$ side, the initial state is $|0\rangle$, and the conductance lines are results of the $|0\rangle \rightarrow |1\rangle$ transitions. In contrast, the $V_g > 0$ side represents the $|1\rangle \rightarrow |0\rangle$ transitions. In the following we will discuss the factors that could partly break the symmetry of the stability diagrams. The unique signature for each type of asymmetric diagram will be given, which could be helpful for the understanding and interpretation of experimental results.

In practice, both the *external* properties such as the electrode-molecule coupling strength (γ^L and γ^R) and the bias coupling constant α and the *intrinsic* properties of the molecule itself such as the frequency difference between the two charging states, the anharmonicity of the PESs, and the vibrational mode-mixing effect [18] could break the symmetry of the stability diagrams. Some of these properties, especially the intrinsic molecular properties, have been studied in previous works. These effects will also be examined here to discuss specifically the corresponding effect on the shape of the stability diagrams.

A. Effect of the external factors

We start the discussion by examining the effect of the external factors on the charge transport properties of the model molecular transistor. The effect of changing the bias coupling constant α and the electrode-molecule coupling strength (γ^L and γ^R) will be discussed in this section.

1. Bias coupling constant α

We first study the effect of the bias coupling constant α on the conductance stability diagrams by keeping all of the other parameters the same as used in the calculation of Fig. 1(c). As shown in Fig. 1(b), α controls the bias drop of the two electrodes; deviation of α from 0.5 can lead to uneven potential energy changes in the two electrodes. It is thus expected that the changes in α could have significant influence on the conductance stability diagram of the transistor. The simulation results for different bias coupling constants are shown in Fig. 2. Compared with Fig. 1(c), the conductance stability diagrams for uneven bias coupling constants have two distinctive features. The first is that the diamond structure becomes tilted with reduced angles between the originally perpendicular conductance lines. The other is that the conductances are no longer symmetric with respect to both the gate and bias voltages. However, we can see that there is still a rotational symmetry around the crossing point of the diamond structure. These features are the direct result of the uneven

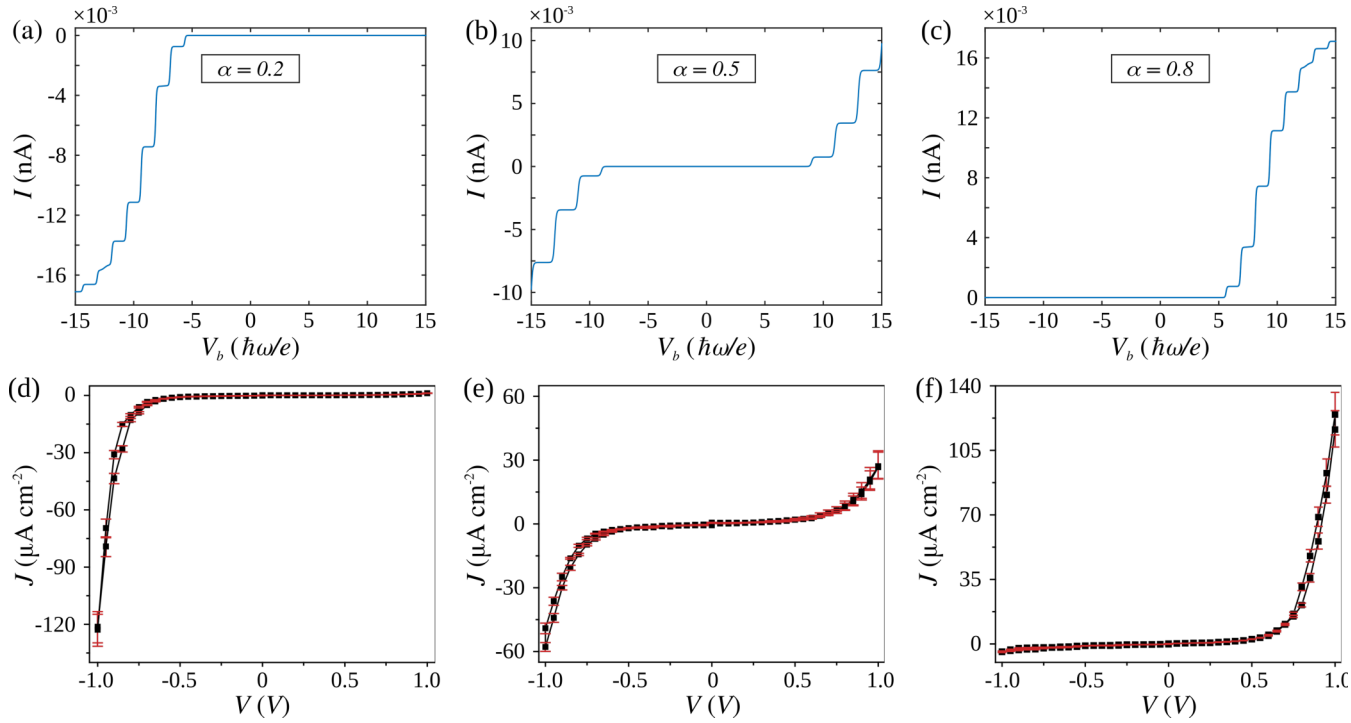

FIG. 3. I-V_b curves calculated at three different bias coupling constants under $V_g = -9\hbar\omega/e$: (a) $\alpha = 0.2$, (b) $\alpha = 0.5$, and (c) $\alpha = 0.8$. The changes in the conductance in (a) and (c) are indicated by the vertical dashed lines in Figs. 2(c) and 2(g), respectively. (d)–(f) The experimental results from Ref. [19]. The experimental results were obtained by tuning the length of the linker groups (alkyl chains) between the conducting unit of the molecule and the electrodes.

bias voltages [with a ratio of $\alpha/(1-\alpha)$ for the left and right electrodes] needed to excite the same group of vibrational energy levels.

In addition, the strong asymmetry of the charge transport properties with respect to the bias voltage caused by the uneven bias drop also leads to clear current rectifications, as can be seen in Fig. 2. Moreover, we can see that by changing α from less than 0.5 to larger than 0.5, there is a reverse of the direction for the current rectification. Interestingly, a recent experiment by Yuan *et al.* successfully realized the control of rectification directions of molecular junctions by changing the length of the linker groups (alkyl chains) between the conducting unit and the electrodes [19]. In their experiment, the effect of changing the length of the linker groups is mainly the changes to the potential drops on the two electrodes, which are equivalent to tuning the bias coupling constant α. This is reasonable since changing the length of the linker groups can affect the electrode capacitances C_L and C_R, and a result of the uneven electrode capacitances is that α will no longer be 0.5. We compare the experimental results with the current-voltage (I-V) characteristics simulated with different α in Fig. 3. As can be seen, the simulation results show very good qualitative agreement with the measured I-V curves, which thus confirms the origin of the current rectification and the changes in the rectification directions are a result of the different bias couplings between the conducting molecule and the two electrodes. It should be mentioned that the experiments were performed on self-assembled monolayers, while the calculations were done for a single molecule with predefined parameters, which is the reason for the large differences between the absolute values of the currents.

2. *Molecule-electrode coupling strength γ*

The molecule-electrode coupling strength is another factor that could lead to asymmetric charge transport in molecular junctions [28]. It is a measure of the bare tunneling rates for the electrons in the electrodes to the molecule and determines the absolute values of the electric current through the molecular transistor. In fact, the currents are proportional to the coupling strength between the molecule and the electrodes. Under the high-bias-voltage limit, the saturation current (the current becomes saturated when all of the conductance channels enter the potential window) for a junction with a symmetric bias coupling constant ($\alpha = 0.5$) can be computed analytically as [14]

$$I_s^{\pm} = \pm|e|\frac{\gamma^L\gamma^R}{\gamma^L+\gamma^R}. \tag{13}$$

From Eq. (13) we can see that changes to either γ^L or γ^R could lead to changes to the magnitude of the saturation current. However, the saturation currents obtained under positive and negative bias voltages will still be the same even with asymmetric coupling strengths. Such a feature is different with the asymmetric bias coupling constants, which could lead to strongly asymmetric saturation currents and thus current rectifications as we discussed above. In order to obtain a clear picture of the influence of γ on the detailed charge transport properties of the model transistor, we have computed the conductance stability diagrams with asymmetric coupling strengths between the molecule and electrodes. The simulation results are shown in Fig. 4.

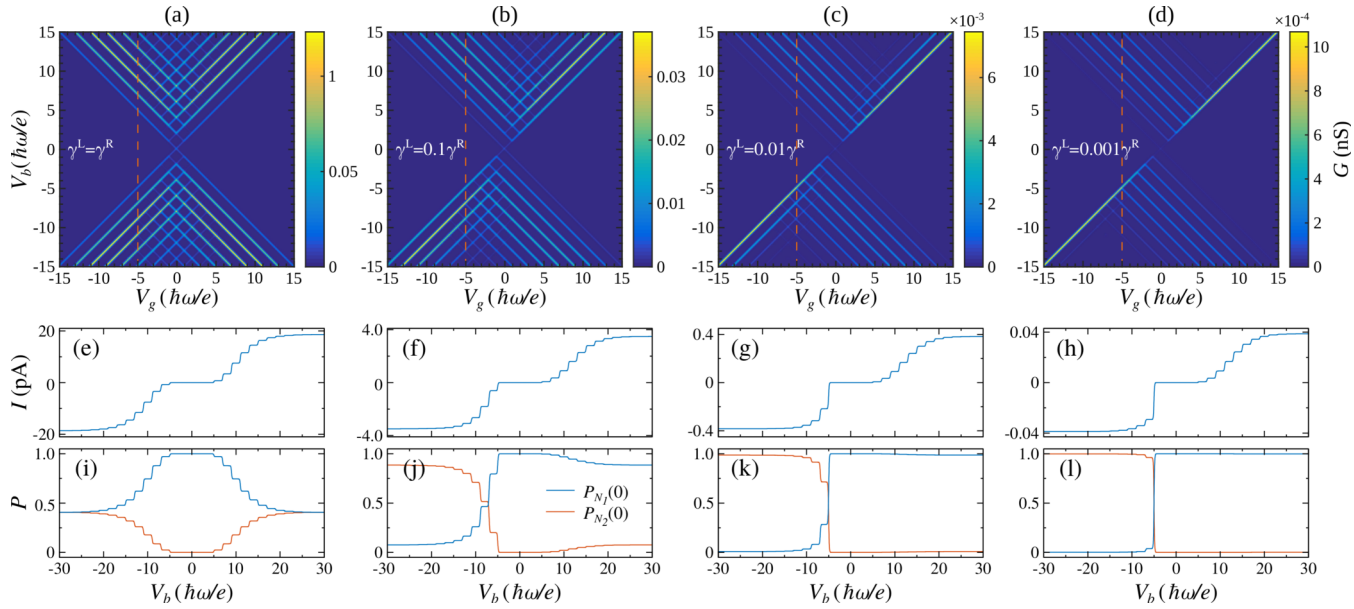

FIG. 4. (a)–(d) Conductance stability diagrams calculated with different values of γ^L. (e)–(h) I-V_b curves with $V_g = -5\hbar\omega/e$. (i)–(l) Steady-state population of the ground vibrational energy level in the two electronic states at $V_g = -5\hbar\omega/e$ as a function of the bias voltage. All of the other parameters are the same as in Fig. 1(c).

As can be found in Figs. 4(a)–4(d), breaking the balance between γ^L and γ^R can also cause the conductance stability diagrams to become asymmetric with respect to both the gate and bias voltages. A rotational symmetry with respect to the degeneracy point can be found which is similar to the case of asymmetric bias coupling constants. However, in this case there are no changes to the angle between the crossing conductance lines which can be used to distinguish the asymmetries caused by the bias coupling constants and the molecule-electrode couplings. Moreover, compared with the changes caused by changing the bias coupling constants, changing the molecule-electrode couplings can lead to much stronger changes to the magnitude of the conductance, as clearly illustrated in Figs. 4(a)–4(d).

Another interesting feature that results from decreased molecule-electrode couplings is the reduced number of conductance lines parallel to the diagonal direction. A clear increase in the conductance to the first conductance line (corresponding to the first conductance peak in G-V_b curves) is also evident. In order to understand such changes, we plot the I-V_b curves and the steady-state populations of the ground vibrational energy levels in the two electronic states obtained at $V_g = -5\hbar\omega/e$ in Figs. 4(e)–4(h) and Figs. 4(i)–4(l), respectively. From the I-V_b curves we see that the shape of the current steps remains almost unchanged under the positive bias voltages. This is due to the similar trends of the population changes at positive bias voltages, as can be seen in Figs. 4(i)–4(l). For the case with the negative bias voltages, on the other hand, there is a sudden change in the populations at the on-site bias voltages ($V_b = -5\hbar\omega/e$). Especially, for the strongly asymmetric case of $\gamma^L = 0.001\gamma^R$, the molecule is almost instantly excited to the final state $|1\rangle$ once the first conductance channel enters the bias window. Such strong changes in the populations are caused by the uneven molecule-electrode couplings which reduce the deexcitation from the left electrode. As a result, the current also undergoes a sudden increase and reaches the saturation values much faster than that of the positive bias voltages, which is responsible for the observed asymmetries in the conductance stability diagrams. The asymmetric I-V_b characteristics shown in Figs. 4(e)–4(h) agree well with the calculations by Härtle and Thoss [28].

B. Effect of the internal factors

So far we have discussed the effect of the external factors on the charge transport properties of the model molecular transistor. In the following we start to investigate the effect of the intrinsic molecular properties, including the shape of the PESs and the mode-mixing effect on the transport properties of the transistor. It should be mentioned that several previous works have also studied the effect of the intrinsic molecular properties such as the vibrational anharmonicity effect [18,29–32] and the charge-state-dependent vibrational frequencies [24,29] on the charge transport properties. However, detailed investigations on these internal factors on the conductance stability diagrams are still desirable to understand the different types of asymmetries that could be observed experimentally.

1. Frequency differences

We first examine the frequency differences between the two electronic states on the transport properties of the transistor. To obtain the signatures of the frequency changes, we will still work with harmonic potentials and assume symmetric bias couplings (by setting α to 0.5) and symmetric molecule-electrode couplings ($\gamma^L = \gamma^R$). The simulation results with $\omega_2 = \omega_1$ and $\omega_2 = 1.2\omega_1$ are shown in Figs. 5(a) and 5(b), respectively. Here the symmetric case of $\omega_1 = \omega_2$ is included for comparison.

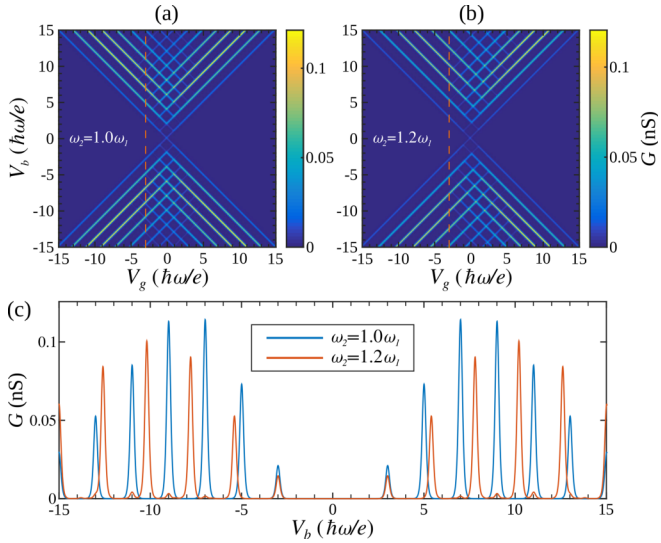

FIG. 5. Effect of frequency changes on the conductance stability diagrams: (a) $\omega_2 = \omega_1$ and (b) $\omega_2 = 1.2\omega_1$. (c) The G-V_b curves obtained with $V_g = -3\hbar\omega/e$. In the simulations α has been set to 0.5. The molecule-electrode coupling has also been set to be symmetric with $\gamma^L = \gamma^R$.

By comparing the diagrams in Figs. 5(a) and 5(b), it can be seen that the space between adjacent conductance lines in the left part of Fig. 5(b) has increased significantly as a result of the increased frequency of the $|1\rangle$ state ω_2. However, the other part of the diagram remains largely unchanged and possesses a shape similar to that of the one obtained with equal frequencies. As a result, the conductance stability diagram is no longer symmetric with respect to the gate voltage. On the other hand, the symmetry with respect to the bias voltages remains which can be applied to distinguish with the asymmetric charge transport properties caused by the external factors. Figure 5(c) shows the G-V_b curves for the two cases at $V_g = -3\hbar\omega/e$. From Fig. 5(c) we can clearly see the increase in the spacing between the adjacent conductance peaks for the result obtained with $\omega_2 = 1.2\omega_1$. It is worth mentioning here that the bias voltage between two adjacent conductance peaks is two times that corresponding to the vibrational frequencies ($\Delta V_b = 2\hbar\omega_2/e$) because $\alpha = 0.5$.

2. *Vibrational anharmonicity effect*

In the study of vibrational excitations in molecular junctions, the most commonly adopted approximation is the harmonic approximation. The harmonic approximation is generally a very good approximation, especially for vibrational modes with higher energy and when only the lower vibrational levels are considered. However, there are situations where a large number of vibrational quanta are required. An important example can be found when dealing with charge transport in the so-called Franck-Condon blockade [15] region where charge transport is mainly contributed by higher vibrational energy levels. For such cases, the vibrational anharmonicity effect could play an important role [18,30]. To this end, we also studied the effect of the anharmonicity on the charge transport properties of the model transistor.

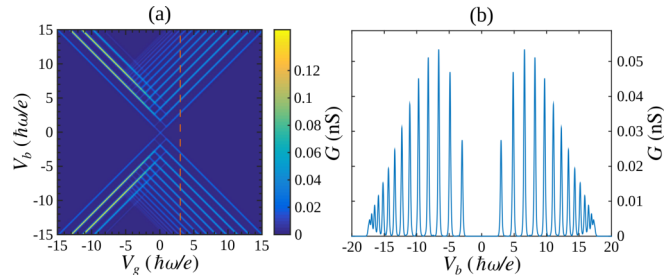

FIG. 6. (a) Conductance stability diagram computed for the model transistor with the Morse potential. (b) G-V_b curve obtained with $V_g = 3\hbar\omega/e$. All of the other parameters are the same as in Fig. 1(c).

In the simulations, the harmonic potential is replaced by the Morse potential to describe the anharmonicity effect. All of the other parameters have been chosen to be the same as those used in the simulation in Fig. 1(c). The simulated conductance stability diagram and the G-V_b curve calculated at $V_g = 3\hbar\omega/e$ are shown in Figs. 6(a) and 6(b), respectively. From Fig. 6(a), it can be seen that the conductance stability diagram also becomes asymmetric with respect to the gate voltage, which is similar to that of the frequency changes. However, unlike in the case of the frequency changes, the asymmetry caused by the vibrational anharmonicity effect is a result of the asymmetric nature of the potential energy surface. We can also find an evident difference between the asymmetries caused by the frequency changes and the vibrational anharmonicity effect, which is the energy spacings between adjacent conductance lines are no longer constant for the latter case. For the Morse potential, the energy for a given vibrational level can be computed as [33]

$$E_n = \left(n + \frac{1}{2}\right)\left[\hbar\omega - \left(n + \frac{1}{2}\right)\frac{\hbar^2\omega^2}{4D}\right], \tag{14}$$

where D is the dissociation energy. The value of D also determines the number of bound levels in the well of the Morse potential with $j = \lceil 2D/\hbar\omega - 1/2\rceil + 1$, where $\lceil\cdot\rceil$ indicates the integer part. We have considered 15 levels ($j = 15$) to be bounded in the simulations. From Eq. (14), we can get the energy spacing between adjacent vibrational levels for the Morse potential as

$$E_{n+1} - E_n = \hbar\omega - (n+1)\frac{\hbar^2\omega^2}{2D}. \tag{15}$$

From Eq. (15) we can see that the energy spacing undergoes gradual decreases together with the increase in the vibrational quantum number n. The reduced energy spacings are clearly illustrated by the G-V_b curves shown in Fig. 6(b).

3. *Mode-mixing effect*

Other than the two factors considered above, the vibrational mode-mixing effect, which is caused by the rotation between the normal coordinates of the two electric states [34–36], could also affect the charge transport properties of a molecular junction [18]. In order to study such an effect, we have considered minimal two-dimensional PESs. The two sets of PESs are assumed to relate to each with a linear

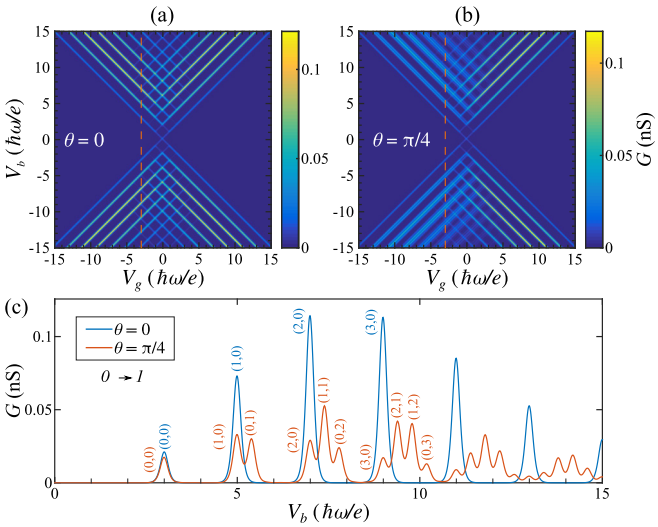

FIG. 7. Conductance stability diagrams simulated with different rotation angles: (a) $\theta = 0$ and (b) $\theta = \pi/4$. (c) The G-V_b curves obtained at $V_g = -3\hbar\omega/e$. The detailed transition assignments are marked beside the peak position. Two vibrational modes with frequencies of 1000 and 1200 cm^{-1} are included in each of the two electronic states. $\Delta Q_1 = 41.90$ a.u., $\Delta Q_2 = 0$. All other parameters are the same as in Fig. 1(c).

transformation as [34]

$$Q_1 = JQ_2 + K. \tag{16}$$

Here Q_1 and Q_2 represent the normal coordinates of the $|0\rangle$ and $|1\rangle$ states, respectively. J is a 2×2 rotation matrix defined by a rational angle θ and K, which is a two-dimensional vector with displacements between the two vibrational modes. In the simulations, the frequencies of the two modes are set to be $\omega_{1,1} = \omega_{2,1} = 1000\ \text{cm}^{-1}$ and $\omega_{1,2} = \omega_{2,2} = 1200\ \text{cm}^{-1}$. Here we use the second number in the subscript to indicate the index of the two modes in the same electric state. For the sake of simplification, we assume only one of the two vibrational modes is Franck-Condon active with $\Delta Q_1 = 41.90$ a.u. The displacement for the other mode has been set to $\Delta Q_2 = 0$. All of the other parameters are the same as in Fig. 1(c). With such a setup, the charge transport process will be solely determined by the Franck-Condon active mode when no mode mixing is considered.

Figures 7(a) and 7(b) are the simulation results with $\theta = 0$ and $\theta = \pi/4$, respectively. As we mentioned above, with $\theta = 0$ (i.e., without the mode-mixing effect), the conductance stability diagram is exactly the same as the one shown in Fig. 1(c) because only one mode is active in this case. When the mode-mixing effect is included, on the other hand, we can again find that the stability diagram no longer has mirror symmetry with respect to the gate voltage. It can be found that the number of conductance lines increased significantly in the negative-gate-voltage part. In contrast, the positive-gate part of the diagram is almost the same as the one without the mode-mixing effect. In order to analyze in detail the changes in the conductance stability diagram caused by the mode-mixing effect, the G-V_b curves for the two cases obtained at $V_g = -3\hbar\omega/e$ are shown in Fig. 7(c). From there we can see that each of the conductance peaks except the first peaks at positive and negative bias voltages in the case of $\theta = 0$ has been replaced by several smaller peaks. The emergence of the additional peaks is due to the involvement of the high-energy modes caused by the mixing of the two modes. In fact, the number of conductance peaks is determined by the possible combinations for a given vibrational quantum number [the detailed assignment for each peak can be found in Fig. 7(c)]. This is a feature that can be applied to distinguish the mode-mixing effect from the other two intrinsic molecular properties.

IV. SUMMARY

In summary, we have performed a systematic study of the effect of various factors that could affect the charge transport properties of weakly coupled molecular junctions. Especially, the effect of both the external factors, including the bias coupling constant and the molecule-electrode coupling constants, and the intrinsic molecular properties such as charge-state-dependent frequencies, vibrational anharmonicity, and the vibrational mode-mixing effect on the conductance stability diagram of a model single-molecule transistor has been investigated in detail. These results show that the external factors and the intrinsic molecular properties can affect the charge transport properties of the transistor in distinctive manners. Both the asymmetric bias and molecule-electrode couplings can cause the conductance stability diagram to be asymmetric with respect to both the bias and gate voltages. In contrast, the intrinsic molecular properties can only lead to asymmetries with respect to the gate voltage. The difference between each of the factors has also been discussed, which could be helpful in the interpretation of experimental results.

Moreover, we also showed that asymmetric bias coupling constants can lead to strong current rectifications as a result of the unbalanced bias voltage drop on the two electrodes. The theoretical results were compared to the experimental results by Yuan *et al.* [19] and were used to explain the change in rectification directions of molecular diodes in the experiments.

ACKNOWLEDGMENTS

This work was supported by the National Natural Science Foundation of China (Grants No. 21603185 and No. 21773169), the "100 Talents Project" of Hebei Province (Grant No. E2016100003), the Natural Science Foundation of Hebei Province (Grant No. B2017203143), and the Science Foundation for the Youth Top-notch Talent from Universities of Hebei Province (Grant No. BJ2017040).

[1] M. L. Perrin, E. Burzuri, and H. S. J. van der Zant, Chem. Soc. Rev. **44**, 902 (2015).

[2] S. Datta, *Quantum Transport: Atom to Transistor* (Cambridge University Press, Cambridge, 2005).

[3] R. Gaudenzi, M. Misiorny, E. Burzurí, M. R. Wegewijs, and H. S. van der Zant, J. Chem. Phys. **146**, 092330 (2017).
[4] Y. Komoto, S. Fujii, M. Iwane, and M. Kiguchi, J. Mater. Chem. C **4**, 8842 (2016).
[5] J. Martínez-Blanco, C. Nacci, S. C. Erwin, K. Kanisawa, E. Locane, M. Thomas, F. Von Oppen, P. W. Brouwer, and S. Fölsch, Nat. Phys. **11**, 640 (2015).
[6] S. W. Wu, G. V. Nazin, X. Chen, X. H. Qiu, and W. Ho, Phys. Rev. Lett. **93**, 236802 (2004).
[7] E. Burzurí, Y. Yamamoto, M. Warnock, X. Zhong, K. Park, A. Cornia, and H. S. van der Zant, Nano Lett. **14**, 3191 (2014).
[8] C. S. Lau, H. Sadeghi, G. Rogers, S. Sangtarash, P. Dallas, K. Porfyrakis, J. Warner, C. J. Lambert, G. A. D. Briggs, and J. A. Mol, Nano Lett. **16**, 170 (2016).
[9] L. H. Yu, Z. K. Keane, J. W. Ciszek, L. Cheng, M. P. Stewart, J. M. Tour, and D. Natelson, Phys. Rev. Lett. **93**, 266802 (2004).
[10] D.-H. Chae, J. F. Berry, S. Jung, F. A. Cotton, C. A. Murillo, and Z. Yao, Nano Lett. **6**, 165 (2006).
[11] E. Osorio, K. O'Neill, N. Stuhr-Hansen, O. Nielsen, T. Bjørnholm, and H. van der Zant, Adv. Mater. **19**, 281 (2007).
[12] E. A. Osorio, T. Bjørnholm, J.-M. Lehn, M. Ruben, and H. S. J. van der Zant, J. Phys. Condens. Matter **20**, 374121 (2008).
[13] R. Leturcq, C. Stampfer, K. Inderbitzin, L. Durrer, C. Hierold, E. Mariani, M. G. Schultz, F. Von Oppen, and K. Ensslin, Nat. Phys. **5**, 327 (2009).
[14] E. Bonet, M. M. Deshmukh, and D. C. Ralph, Phys. Rev. B **65**, 045317 (2002).
[15] J. Koch and F. von Oppen, Phys. Rev. Lett. **94**, 206804 (2005).
[16] J. S. Seldenthuis, H. S. Van Der Zant, M. A. Ratner, and J. M. Thijssen, ACS Nano **2**, 1445 (2008).
[17] G. Tian and Y. Luo, J. Phys. Chem. C **118**, 14853 (2014).
[18] G. Tian, S. Duan, G.-P. Zhang, W. Hu, and Y. Luo, Phys. Chem. Chem. Phys. **17**, 23007 (2015).
[19] L. Yuan, N. Nerngchamnong, L. Cao, H. Hamoudi, E. Del Barco, M. Roemer, R. K. Sriramula, D. Thompson, and C. A. Nijhuis, Nat. Commun. **6**, 6324 (2015).
[20] J. M. Thijssen and H. S. J. van der Zant, Phys. Status Solidi B **245**, 1455 (2008).
[21] K. Stokbro, J. Phys. Chem. C **114**, 20461 (2010).
[22] M. Leijnse and M. R. Wegewijs, Phys. Rev. B **78**, 235424 (2008).
[23] H. Hübener and T. Brandes, Phys. Rev. B **80**, 155437 (2009).
[24] B. Dong, H. Y. Fan, X. L. Lei, and N. J. M. Horing, J. Appl. Phys. **105**, 113702 (2009).
[25] T. E. Sharp and H. M. Rosenstock, J. Chem. Phys. **41**, 3453 (1964).
[26] P. Johansson, H. Xu, and M. Käll, Phys. Rev. B **72**, 035427 (2005).
[27] G. Tian, S. Duan, W. Hua, and Y. Luo, DYNAVIB, version 1.0, Royal Institute of Technology, Stockholm, 2012.
[28] R. Härtle and M. Thoss, Phys. Rev. B **83**, 115414 (2011).
[29] J. Koch and F. von Oppen, Phys. Rev. B **72**, 113308 (2005).
[30] F. Elste and F. von Oppen, New J. Phys. **10**, 065021 (2008).
[31] D. Brisker and U. Peskin, J. Chem. Phys. **125**, 111103 (2006).
[32] H. M. Friedman, B. K. Agarwalla, and D. Segal, J. Chem. Phys. **146**, 092303 (2017).
[33] P. Morse, Phys. Rev. **34**, 57 (1929).
[34] F. Duschinsky, Acta Physicochim. URSS **7**, 551 (1937).
[35] A. Mebel, M. Hayashi, K. Liang, and S. Lin, J. Phys. Chem. A **103**, 10674 (1999).
[36] Q. Peng, Y. Yi, Z. Shuai, and J. Shao, J. Am. Chem. Soc. **129**, 9333 (2007).